

# Neural networks built from enzymatic reactions can operate as linear and nonlinear classifiers

Christian Cuba Samaniego<sup>1</sup>, Emily Wallace<sup>2</sup>, Franco Blanchini<sup>3</sup>, Elisa Franco<sup>4</sup>, Giulia Giordano<sup>5</sup>

**Abstract**—The engineering of molecular programs capable of processing patterns of multi-input biomarkers holds great potential in applications ranging from in vitro diagnostics (e.g., viral detection, including COVID-19) to therapeutic interventions (e.g., discriminating cancer cells from normal cells). For this reason, mechanisms to design molecular networks for pattern recognition are highly sought after. In this work, we explore how enzymatic networks can be used for both linear and nonlinear classification tasks. By leveraging steady-state analysis and showing global stability, we demonstrate that these networks can function as molecular perceptrons, fundamental units of artificial neural networks—capable of processing multiple inputs associated with positive and negative weights to achieve linear classification. Furthermore, by composing orthogonal enzymatic reactions, we show that multi-layer networks can be constructed to achieve nonlinear classification.

Biomolecular Neural Networks, Molecular sequestration, Chemical reactions, Enzymatic network, Biological systems.

## I. INTRODUCTION

Cellular decision-making encompasses various endogenous processes that determine the fate of cells, whether they should replicate, differentiate, or undergo cell death. For example, apoptosis describes processes associated with programmed cell death to eliminate cells that are classified as abnormal or unnecessary cells. In embryonic development, individual cells process multiple environmental cues to decide whether they should differentiate, migrate, or decay. We are only beginning to understand the underlying mechanisms and factors influencing these crucial cellular decisions, which depend on a multitude of factors. Recent work has put forward the intriguing hypothesis that cellular decision making may present similarities with classification tasks performed by Artificial Neural Networks [1]–[4].

Theoretical work has illustrated that biochemical networks including sequestration or phosphorylation reactions can approximate ideal Artificial Neural Networks (ANNs) for linear and nonlinear classifiers [3], [4]. Experimental, bottom-up

implementations of classifiers using biological molecules have been recently proposed in vitro, based on DNA strand displacement [5], and using the enzymatic PEN toolbox, leading to the demonstration of nonlinear classifiers [6]. In bacteria, synthetic genetic circuits based on transcription factors can generate diverse patterns [1], while metabolic networks can implement linear classifiers [7]. In mammalian cells, sequestration-based and phosphorylation-based nonlinear classifiers have been demonstrated [8], [9]; further, protein-based linear classifiers based on the “winner-takes-all” principle have also been built [10].

Here, we examine a new set of biomolecular programs based on enzymatic association and degradation to build a biomolecular classifier. We take inspiration from the architecture of classifiers in ANNs, which are based on the interconnection of simple fundamental units known as “perceptrons”. A molecular perceptron requires only two core species, an enzyme and its substrate. The species producing enzyme and substrate serve as inputs to the perceptron. Through a rigorous steady-state analysis, we establish that our perceptrons operate robustly and generate classifiers with a linear *decision boundary* (namely, the hyper-surface that separates data points belonging to different classification labels), as long as enzyme-substrate association is sufficiently fast. Through computational simulations we then illustrate how the interconnection of multiple perceptrons with linear decision boundaries produces nonlinear classifiers. The simple enzymatic reactions we adopt expand the repertoire of available systems that can generate classifiers.

## II. A MOLECULAR PERCEPTRON

A perceptron is the fundamental unit of ANNs. Perceptrons process a weighted sum of their inputs, which is fed into activator functions, for example ReLU (Rectified Linear Unit) activation functions. In this section, we propose an enzymatic reaction that asymptotically can behave as a molecular perceptron. Although concentrations and rate constants are always positive, the network we propose can process multiple inputs associated with positive and negative weights. We provide a thorough analysis of the perceptron module dynamics, and in particular we show that the trajectories are bounded, and that the system admits an equilibrium that is structurally globally asymptotically stable.

### A. Chemical reactions and ODE model

In the following we denote chemical species with uppercase letters (e.g.  $X$ ) and their concentrations with the corresponding lowercase letters ( $x$ ). An enzymatic perceptron (Fig. 1A) consists of two species,  $Y$  (substrate) and  $Z$

<sup>1</sup> Department of Computational Biology, Carnegie Mellon University, Pittsburgh, PA, USA

<sup>2</sup> Michigan University, Ann Arbor, MI, USA

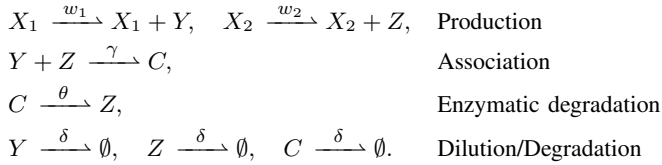
<sup>3</sup> Department of Mathematics, Computer Science and Physics, University of Udine, Italy.

<sup>4</sup> Department of Mechanical and Aerospace Engineering, University of California, Los Angeles, CA, USA.

<sup>5</sup> Department of Industrial Engineering, University of Trento, Italy.

The work of G. Giordano was funded by the European Union through the ERC INSPIRE grant (project number 101076926); views and opinions expressed are however those of the authors only and do not necessarily reflect those of the European Union or the European Research Council; neither the European Union nor the granting authority can be held responsible for them.

(enzyme). Free (unbound) enzyme  $Z$  binds to the substrate  $Y$ , forming the enzyme-substrate complex  $C$ , at rate constant  $\gamma$ . This complex  $C$  catalyzes the degradation of  $Y$ , while  $Z$  dissociates from the complex, releasing free enzyme. The catalytic step (and release of  $Z$ ) occurs at rate constant  $\theta$ . Two inputs  $X_1$  and  $X_2$  produce respectively the species  $Y$  and  $Z$  at rate constants  $w_1$  and  $w_2$ . We assume that all the species  $Y$ ,  $Z$  and  $C$  dilute/degrade with rate constant  $\delta$  as shown in Fig. 1A. Overall, our proposed enzymatic perceptron module is described by the following chemical reactions:



The association between enzyme and substrate is a second order reaction akin to molecular association [3], [11]–[13]. We will discuss the key role played by the related reaction rate parameter  $\gamma$  in guaranteeing desirable properties of this network.

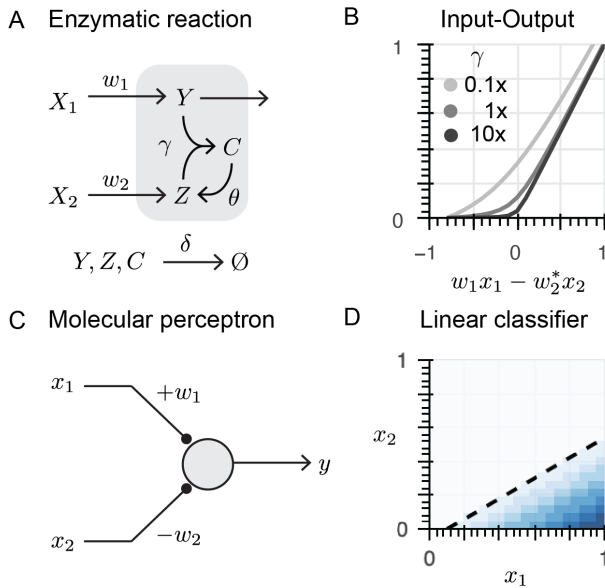


Fig. 1. A: Reaction network describing the enzymatic perceptron. B: The input-output curve for different values of  $\gamma$  computes a ReLU activation function;  $w_2^* = (1 + \theta/\delta)w_2$ . C: Schematic of the general architecture of a perceptron. D: At steady-state, the enzymatic perceptron realizes a linear classifier with a decision boundary corresponding to the black dashed line.

Based on the law of mass action, we can write the corresponding system of Ordinary Differential Equations (ODEs) to describe the time evolution of the species concentrations:

$$\dot{y} = w_1 x_1 - \delta y - \gamma y z, \quad (1)$$

$$\dot{z} = w_2 x_2 - \delta z - \gamma y z + \theta c, \quad (2)$$

$$\dot{c} = \gamma y z - \delta c - \theta c. \quad (3)$$

We now examine the stability properties of this circuit.

### B. Steady-state analysis in a fast association regime

We will show that as long as the enzyme/substrate association constant  $\gamma$  is sufficiently large, the system (1)-(3) asymptotically operates as a perceptron. In other words, this system

processes the weighted sum of input  $x_1$  (associated with a positive weight) and input  $x_2$  (associated with a negative weight) to generate a piecewise linear function that is equal to the difference of the weighted sum, if the difference is non-negative, and zero otherwise. This operation is equivalent to a ReLU activation function.

Let us compute the equilibria of system (1)-(3). By setting equation (3) to zero, we have:

$$\bar{c} = \frac{\gamma}{\delta + \theta} \bar{y} \bar{z}. \quad (4)$$

Then,  $\bar{z}$  is obtained by setting both equations (1) and (2) to zero:

$$\bar{z} = \frac{w_1 x_1 - \delta \bar{y}}{\gamma \bar{y}} = \frac{w_2 x_2}{\gamma \frac{\delta}{\theta + \delta} \bar{y} + \delta}. \quad (5)$$

We thus obtain the second order polynomial

$$A \bar{y}^2 + B \bar{y} + C = 0, \quad (6)$$

where

$$\begin{aligned} A &= \frac{\delta}{\theta + \delta}, \\ B &= \frac{1}{\delta} \left[ w_2 x_2 - \frac{\delta}{\theta + \delta} w_1 x_1 \right] + \frac{\delta}{\gamma}, \\ C &= -\frac{w_1 x_1}{\gamma}. \end{aligned}$$

Since  $A > 0$  and  $C < 0$ , equation (6) admits a single positive real solution, which is:

$$\bar{y} = \frac{-B + \sqrt{B^2 - 4AC}}{2A}. \quad (7)$$

Relying on approximations that are valid in the fast association regime (i.e.,  $\gamma$  arbitrarily large), we can consider the following approximated steady-state value for  $y$ :

$$\lim_{\gamma \rightarrow \infty} \bar{y} = \frac{1}{\delta} \max \left\{ 0, w_1 x_1 - \left( 1 + \frac{\theta}{\delta} \right) w_2 x_2 \right\}. \quad (8)$$

In fact, by defining  $L := \lim_{\gamma \rightarrow \infty} -B/A$  and  $M := 4w_1 x_1 (\theta + \delta)/\delta$ , we have

$$\lim_{\gamma \rightarrow \infty} \bar{y} = \lim_{\gamma \rightarrow \infty} \frac{L + \sqrt{L^2 + M/\gamma}}{2} = \begin{cases} 0 & \text{if } L \leq 0 \\ L & \text{if } L > 0 \end{cases}$$

with

$$\begin{aligned} L &= \lim_{\gamma \rightarrow \infty} \frac{1}{\delta} \left[ w_1 x_1 - \left( 1 + \frac{\theta}{\delta} \right) w_2 x_2 - \frac{(\delta + \theta)\delta}{\gamma} \right] \\ &= \frac{1}{\delta} \left[ w_1 x_1 - \left( 1 + \frac{\theta}{\delta} \right) w_2 x_2 \right]. \end{aligned}$$

Equation (8) resembles the output of a ReLU activation function for two inputs:  $x_1$ , with a positive weight  $+w_1$ , and  $x_2$ , with a negative weight  $-w_2^* = -(1 + \theta/\delta)w_2$ , as shown in Fig. 1B. Decreasing the association rate constant  $\gamma$  makes the input-output response look like a soft-ReLU. When  $\theta = 0$ , the enzyme-substrate association reaction (akin to molecular sequestration) is the core of the system. Therefore, we can abstract our enzymatic network as a molecular perceptron, as shown in Fig. 1 C.

The steady-state input-output map of system (1)-(3) can be computed by evaluating equation (7) when the inputs ( $x_1$  and  $x_2$ ) range from 0 to 1. In the heat plot shown in Fig. 1 D, the white region corresponds to an output close to zero, while the blue range corresponds to an output larger than zero. The black dashed line represent the *decision boundary* that separates the white and blue regions. This computed input-output map is equivalent to a linear classifier, because the decision boundary is a line dividing the input domain in two regions. The system output produces a response larger than zero only when the input combination  $(x_1, x_2)$  falls in the blue region.

We can also find a closed-form expression for the decision boundary (the black dashed line in Fig. 1 D). For this purpose, we rewrite equation (5):

$$w_1 x_1 - \left( \frac{\bar{y}}{\frac{\delta}{\theta+\delta} \bar{y} + \frac{\delta}{\gamma}} \right) w_2 x_2 = \delta \bar{y}. \quad (9)$$

This equation describes the relationship between  $x_1$  and  $x_2$  when  $y$  is constant, as a function of the network reaction rate parameters. Fig. 1 D shows the decision boundary for  $\bar{y} = 0.1$ . In the fast association regime ( $\gamma \rightarrow \infty$ ), the decision boundary becomes:

$$w_1 x_1 - \left( 1 + \frac{\theta}{\delta} \right) w_2 x_2 = \delta \bar{y}.$$

### C. Boundedness and equilibria

All the state variables of system (1)-(3) are bounded, for all possible nonnegative initial conditions, if the inputs  $w_1 x_1 =: \alpha$  and  $w_2 x_2 =: \beta$  are constant and bounded. In fact, since the system is positive (each state variable has a nonnegative derivative when its value is zero),  $y, z, c \geq 0$ . Moreover,

$$\frac{d}{dt}(y+c) = -\delta(y+c) - \theta c + \alpha \leq -\delta(y+c) + \alpha,$$

hence  $y+c$  is bounded, and similarly

$$\frac{d}{dt}(z+c) = -\delta(z+c) - \theta c + \beta \leq -\delta(z+c) + \beta,$$

hence  $z+c$  is bounded. Therefore both  $y$  and  $z$  are bounded, because all the variables are nonnegative. Finally, from (3),  $c$  is also bounded.

Rewriting the dynamics of system (1)-(3), assuming constant inputs, with the new state variables  $v = y+c$ , and  $\zeta = z+c$  yields the ODE system

$$\dot{v} = \alpha - \delta v - \theta c \quad (10)$$

$$\dot{\zeta} = \beta - \delta \zeta \quad (11)$$

$$\dot{c} = \gamma(v-c)(\zeta-c) - (\delta+\theta)c \quad (12)$$

Since  $y, z, c$  are nonnegative variables, we have

$$v-c = y \geq 0 \quad \text{and} \quad \zeta-c = z \geq 0.$$

The system (10)-(12) has bounded solutions, for all possible nonnegative initial conditions with  $c \leq \min\{v, \zeta\}$ . In fact,  $\zeta$  is bounded as it obeys to equation (11); then also  $c$  is

bounded by  $\zeta$ ; and, from equation (10), also  $v$  is bounded, because  $c$  is bounded.

Boundedness implies the existence of an equilibrium [14]–[16]. For system (1)-(3), the equilibrium has been computed in Section II-B. For system (10)-(12), the equilibrium can be computed as follows. First, from (11),  $\bar{\zeta} = \beta/\delta$ . Then, by setting to zero equation (12), we obtain

$$(\bar{v}-\bar{c})(\bar{\zeta}-\bar{c}) = \frac{(\delta+\theta)\bar{c}}{\gamma}. \quad (13)$$

Since  $c$  is bounded by  $\zeta$  regardless of the value of  $\gamma$ , for  $\gamma \rightarrow \infty$  the right-hand-side of equation (13) converges to 0, and hence the limit equation is  $(v-c)(\zeta-c) = 0$ , which means that either  $v-c = 0$  or  $\zeta-c = 0$ . On the other hand, since  $c$  is upper bounded by both  $v$  and  $\zeta$ , for  $\gamma \rightarrow \infty$  the equilibrium becomes

$$\bar{c} = \min\{\bar{v}, \bar{\zeta}\}. \quad (14)$$

Now we can distinguish two cases.

First case: if  $\bar{\zeta} \leq \bar{v}$ , then  $\bar{c} = \bar{\zeta} = \beta/\delta$ .

Second case: if  $\bar{\zeta} > \bar{v}$ , then  $\bar{c} = \bar{v}$ . By setting to zero equation (10), we get

$$0 = \alpha - \delta \bar{v} + \theta \bar{c} = \alpha - \delta \bar{v} + \theta \bar{v}$$

and hence  $\bar{c} = \bar{v} = \alpha/(\delta+\theta)$ .

Therefore, in the fast association regime ( $\gamma \rightarrow \infty$ ),

$$\lim_{\gamma \rightarrow \infty} \bar{c} = \min\left\{ \frac{\alpha}{\delta+\theta}, \frac{\beta}{\delta} \right\} = \min\left\{ \frac{w_1 x_1}{\delta+\theta}, \frac{w_2 x_2}{\delta} \right\}. \quad (15)$$

Then, the equilibrium value for  $v$  in the fast association regime is

$$\begin{aligned} \lim_{\gamma \rightarrow \infty} \bar{v} &= \frac{\alpha}{\delta} - \frac{\theta}{\delta} \lim_{\gamma \rightarrow \infty} \bar{c} \\ &= \max\left\{ \frac{\alpha}{\delta} - \frac{\alpha\theta}{\delta(\delta+\theta)}, \frac{\alpha}{\delta} - \frac{\beta\theta}{\delta^2} \right\} \\ &= \max\left\{ \frac{\alpha}{\delta+\theta}, \frac{\alpha}{\delta} - \frac{\beta\theta}{\delta^2} \right\}. \end{aligned}$$

### D. Stability analysis

We now assess the stability of the equilibrium that we have computed. Since system (10)-(12) is obtained from system (1)-(3) through a linear coordinate transformation, the stability properties of the equilibrium are identical in the two cases.

We start by proving its local asymptotic stability, which holds structurally, i.e., regardless of parameter values [17].

**Proposition 1.** *The equilibrium point of system (10)-(12) (equivalently, of system (1)-(3)) is structurally locally asymptotically stable.*

*Proof.* At steady-state, we have that  $\bar{v}-\bar{c} = \bar{y} \geq 0$  and  $\bar{\zeta}-\bar{c} = \bar{z} \geq 0$ , while  $\bar{c} > 0$ . Therefore, we can prove that the equilibrium  $(\bar{v}, \bar{\zeta}, \bar{c})$  is structurally asymptotically stable [17], regardless of parameter values. Indeed the Jacobian of system (10)-(12) is

$$J = \begin{bmatrix} -\delta & 0 & -\theta \\ 0 & -\delta & 0 \\ \gamma \bar{z} & \gamma \bar{y} & -k \end{bmatrix},$$

where  $k := \gamma\bar{y} + \gamma\bar{z} + (\delta + \theta)$ . Its characteristic polynomial  $\psi(s) = \det(sI - J)$  is Hurwitz, since it can be factored out as  $\psi(s) = (s + \delta) [s^2 + s(\delta + k) + \delta k + \gamma\theta\bar{z}]$ , and therefore all its roots must have a strictly negative real part.  $\square$

We can actually prove *global* stability of the equilibrium, again structurally [17]. Consider again the original representation, which we report here for convenience:

$$\dot{y} = \alpha - \delta y - \gamma y z, \quad (16)$$

$$\dot{z} = \beta - \delta z - \gamma y z + \theta c, \quad (17)$$

$$\dot{c} = \gamma y z - \delta c - \theta c, \quad (18)$$

where  $\alpha$  and  $\beta$  are constant positive inputs. We recall that the shifted variable

$$\zeta := z + c$$

satisfies the differential equation

$$\dot{\zeta} = \beta - \delta \zeta. \quad (19)$$

Hence,  $\zeta$  (namely,  $z + c$ ) exponentially converges to the variety

$$z + c = \frac{\beta}{\delta} \doteq \bar{\zeta}. \quad (20)$$

We can then prove convergence inside this variety. Consider the first two equations and write them as

$$\dot{y} = \alpha - \delta y - \gamma y z, \quad (21)$$

$$\dot{z} = \beta - \delta z - \gamma y z + \theta(\bar{\zeta} - z). \quad (22)$$

Denoting by  $\bar{y}$  and  $\bar{z}$  the equilibrium values corresponding to the given  $\alpha$  and  $\beta$ , we now consider the shifted system in the variables  $p = y - \bar{y}$  and  $q = z - \bar{z}$ :

$$\dot{p} = -\delta p - \gamma g(p, q), \quad (23)$$

$$\dot{q} = -\delta q - \gamma g(p, q) - \theta q, \quad (24)$$

where we denoted  $g(p, q) := (p + \bar{y})(q + \bar{z}) - \bar{y}\bar{z}$ . Since  $g(0, 0) = 0$ , the new system admits the equilibrium  $(p, q) = (0, 0)$ .

To structurally prove global asymptotic stability, we apply the theory developed in [18], [19]. We write

$$g(p, q) = D_p p + D_q q,$$

where  $D_p(p, q)$  and  $D_q(p, q)$  are positive functions; for instance,  $yz - \bar{y}\bar{z} = \bar{z}(y - \bar{y}) + \bar{y}(z - \bar{z}) = \bar{z}p + \bar{y}q$ . Then, the system can be written as

$$\frac{d}{dt} \begin{bmatrix} p \\ q \end{bmatrix} = \begin{bmatrix} -\delta - \gamma D_p & -\gamma D_q \\ -\gamma D_p & -\delta - \gamma D_q - \theta \end{bmatrix} \begin{bmatrix} p \\ q \end{bmatrix} =: H \begin{bmatrix} p \\ q \end{bmatrix}.$$

Since matrix  $H$  is column diagonally dominant and strictly nonsingular, it admits the 1-norm as a Lyapunov function. Therefore, the asymptotic stability of the equilibrium is global, and it is structural since it holds regardless of the values of the positive parameters.

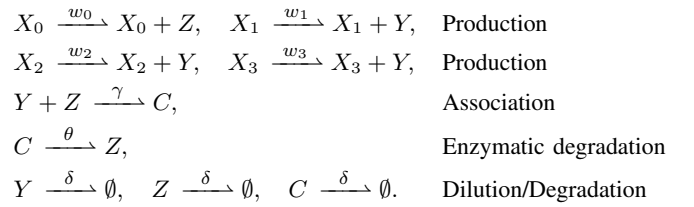
We formalize these results in the following statement.

**Proposition 2.** *For any initial condition and constant positive inputs, and for all values of the positive parameters, the state of system (1)-(3) (equivalently, of (10)-(12)) converges*

*to the affine variety (20). Then, for any initial state in this variety, the system state structurally converges to the (unique) equilibrium. Therefore, the equilibrium is structurally globally asymptotically stable.*

### III. MULTI-INPUT LINEAR CLASSIFIER

In the previous sections we examined a perceptron that achieves linear classification by only processing two inputs  $x_1$  and  $x_2$ . Here, through numerical simulations, we compute the decision boundary for perceptrons with three inputs, as shown in Fig. 2 A. The system now includes three inputs  $X_1, X_2$ , and  $X_3$ , associated with positive weights  $w_1, w_2$ , and  $w_3$ . Each of the inputs produces species  $Y$ . We introduce a *bias* input species  $X_0$ , associated with a negative weight  $w_0$ , which produces species  $Z$ . The association reaction between  $Y$  and  $Z$  is the same as in the two-input perceptron. All species dilute/degrade at the same rate constant  $\delta$ . We list below all the chemical reactions networks, which reflect the abstract design in Fig. 2 A:



Next, using mass conservation, we can write the ODEs:

$$\dot{y} = w_1 x_1 + w_2 x_2 + w_3 x_3 - \delta y - \gamma y z, \quad (25)$$

$$\dot{z} = w_0 x_0 - \delta z - \gamma y z + \theta c, \quad (26)$$

$$\dot{c} = \gamma y z - \delta c - \theta c. \quad (27)$$

Following similar steps as in the perceptron case, we can compute the decision boundary at the steady-state, which for the multi-input linear classifier becomes

$$w_1 x_1 + w_2 x_2 + w_3 x_3 - \frac{\bar{y}}{\frac{\delta}{\theta + \delta} \bar{y} + \frac{\delta}{\gamma}} w_0 x_0 = \delta \bar{y}. \quad (28)$$

Equation (28) describes a plane in the space  $x_1, x_2, x_3$ , assuming large association constant ( $\gamma \rightarrow \infty$ ), as shown in Fig. 2B. When the combination of inputs is located in the right side of the plane, the output is larger than zero. In contrast, when the combination of input corresponds to a point below the plane, the output is zero. By changing the weights of the inputs, we can tune the decision boundary as shown in Fig. 2B.

### IV. NONLINEAR CLASSIFIER

In this section, we report computational simulations that illustrate the behavior of multiple interconnected perceptrons. Through these interconnections, we show that we can create classifiers with nonlinear decision boundaries.

For this purpose, we design a two-layer classifier as shown in Fig. 3 A. The first layer consists of two enzymatic perceptrons, labeled 1 and 2 and represented as gray nodes in the perceptron network in Fig. 3 A and B. The first node process the inputs  $x_1$  and  $x_2$  with positive weight  $w_1^1$  and a negative weight  $w_2^1$  respectively; this node also processes the bias input  $x_0$  with a negative weight  $w_0^1$ . The second node

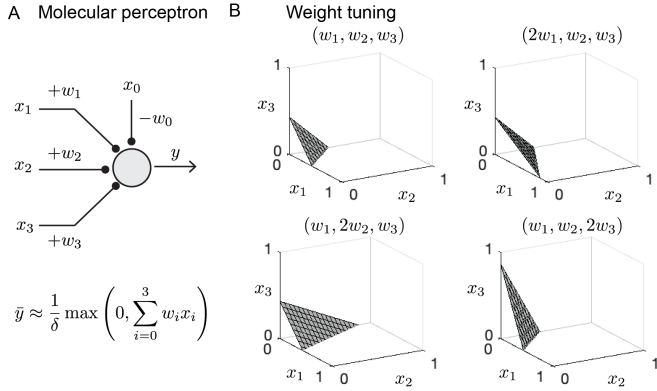


Fig. 2. A: Schematic of a three-input perceptron. B: Simulations showing how the decision boundary depends on the input weights.

takes in the inputs  $x_1$  and  $x_2$  with positive weights  $w_1^2$  and  $w_2^2$ , and it processes the bias input  $x_0$  with a negative weight  $w_0^2$ . The second layer consists of a single node, represented in green in Fig. 3 A and B. So far, we have taken the substrate species  $Y$  as the output of the perceptron. Here, we take the complex  $C$  as the output, and show that we can produce a nonlinear decision boundary based on the outputs of the first layer. In this layer, we remove the enzymatic degradation step, but preserve the molecular association at the core of this node. In fact, from equation (15) we see that in the fast association regime, even when  $\theta = 0$ , the complex output is the minimum of the two inputs, suitably scaled.

Using the reactions represented in the schematic in Fig. 3 B, we can derive the ODEs describing the dynamics of the first node:

$$\dot{y}_1 = w_1^1 x_1 - \delta y_1 - \gamma y_1 z_1, \quad (29)$$

$$\dot{z}_1 = w_0^1 x_0 + w_2^1 x_2 - \delta z_1 - \gamma y_1 z_1 + \theta c_1, \quad (30)$$

$$\dot{c}_1 = \gamma y_1 z_1 - \delta c_1 - \theta c_1. \quad (31)$$

At steady-state, we can find the decision boundary, which is described by the linear equation:

$$(w_1^1 x_1) - \left( \frac{\bar{y}_1}{\frac{\delta}{\theta + \delta} \bar{y}_1 + \frac{\delta}{\gamma}} \right) (w_0^1 x_0 + w_2^1 x_2) = \delta \bar{y}_1. \quad (32)$$

The input-output steady-state map of the first node is shown in Fig. 3 C, left. The decision boundary in Equation (32) is the dashed line separating the blue region from the white area. Similarly, given the schematic in Fig. 3 B we can find the ODEs describing the dynamics of node 2 in layer 1:

$$\dot{y}_2 = w_1^2 x_1 + w_2^2 x_2 - \delta y_2 - \gamma y_2 z_2, \quad (33)$$

$$\dot{z}_2 = w_0^2 x_0 - \delta z_2 - \gamma y_2 z_2 + \theta c_2, \quad (34)$$

$$\dot{c}_2 = \gamma y_2 z_2 - \delta c_2 - \theta c_2. \quad (35)$$

As we did before, we find the equation that describes the decision boundary for the node:

$$(w_1^2 x_1 + w_2^2 x_2) - \left( \frac{\bar{y}_2}{\frac{\delta}{\theta + \delta} \bar{y}_2 + \frac{\delta}{\gamma}} \right) (w_0^2 x_0) = \delta \bar{y}_2. \quad (36)$$

Fig. 3 C, middle, shows the steady-state input-output map of the second node. For both nodes 1 and 2, the computed

decision boundaries separate the white region from the blue region. Input combinations associated with points in the plane above the decision boundary correspond to node outputs larger than zero. In contrast, input combinations associated with points below the decision boundary correspond to an output equal to zero.

Finally, we can write the equations corresponding to the second layer, which includes a single node that has the complex  $c_3$  as an output:

$$\dot{y}_3 = w_1^3 y_1 - \delta y_3 - \gamma y_3 z_3 \quad (37)$$

$$\dot{z}_3 = w_2^3 y_2 - \delta z_3 - \gamma y_3 z_3 \quad (38)$$

$$\dot{c}_3 = \gamma y_3 z_3 - \delta c_3 \quad (39)$$

Resorting to the same derivations as in Section II-C, we find that, in the fast association regime, the output  $c$  computes the minimum of its inputs, suitably scaled, at steady-state. In particular, taking  $\theta = 0$ , equation (15) leads to:

$$\bar{c}_3 = \frac{1}{\delta} \min(w_1^3 \bar{y}_1, w_2^3 \bar{y}_2). \quad (40)$$

Now, by interconnecting the input-output maps of the first layer with the second layer, we can predict the overall output of the classifier. The output of node 3 is the scaled minimum of its two inputs. Therefore, when the output of either node 1 or node 2 is in the white region, the output  $c_3$  is also in the white region. The overall decision boundary for node 3 (i.e., the second layer) can be visualized by overlapping the decision boundaries of nodes 1 and 2 (i.e., the first layer), as shown in Fig. 3 C (right), which yields a nonlinear blue area. Thus, the combination of the linear decision boundaries from the first layer (node 1 and 2) sets the boundaries of the output of the node 3. For this reason, by tuning the individual linear decision boundaries of each node, we can tune the nonlinear decision boundary of the whole network. If the output of node 3 is either the substrate  $y_3$  or the enzyme  $z_3$ , then the classifier retains a nonlinear decision boundary as shown in Fig. 3 D, however its shape can no longer be intuitively mapped to the boundaries of nodes 1 and 2.

TABLE I

TABLE I. PARAMETERS USED IN COMPUTATIONAL SIMULATIONS.

Parameter	Unit	Value	Figure
$\delta$	$\text{h}^{-1}$	1	all
$\theta$	$\text{h}^{-1}$	1	all
$\gamma$	$\mu\text{M}^{-1}\text{h}^{-1}$	100	all
$w_1 = w_2$	$\text{h}^{-1}$	1	Fig. 1
$w_1 = w_2 = w_3$	$\text{h}^{-1}$	1	Fig. 2
$w_0 x_0$	$\mu\text{Mh}^{-1}$	0.6	Fig. 2
$w_1^1 = 2w_2^1$	$\text{h}^{-1}$	1	Fig. 3
$w_0^1 x_0$	$\mu\text{Mh}^{-1}$	0	Fig. 3
$w_1^2 = w_2^2$	$\text{h}^{-1}$	1	Fig. 3
$w_0^2 x_0$	$\mu\text{Mh}^{-1}$	0.4	Fig. 3
$w_1^3 = w_2^3$	$\text{h}^{-1}$	1	Fig. 3
$w_0^3 x_0$	$\mu\text{Mh}^{-1}$	0	Fig. 3

## V. DISCUSSION

We have demonstrated that suitably designed enzymatic reactions can asymptotically give rise to an ideal perceptron implementing a linear classifier, when the association rate is

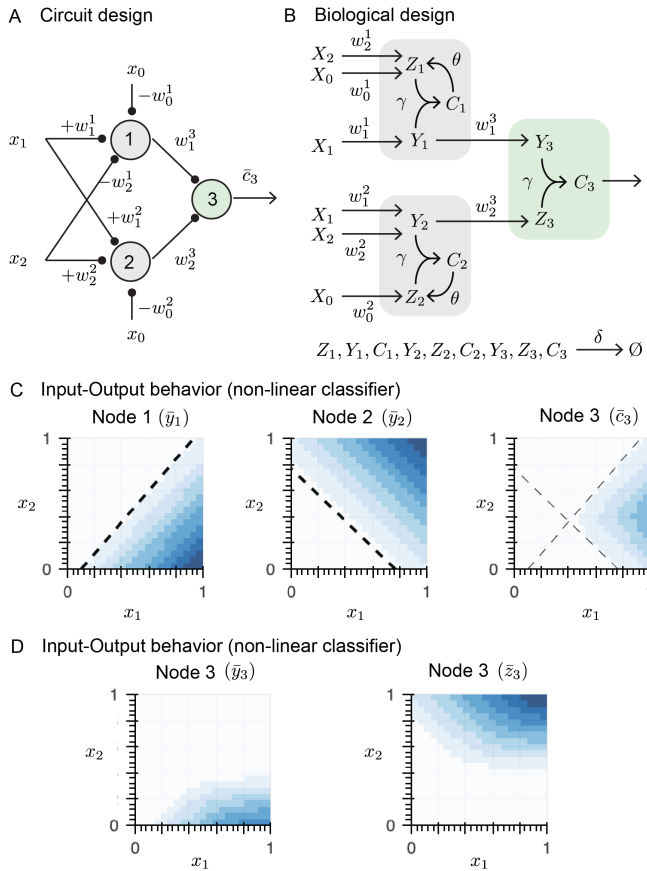


Fig. 3. A: Schematic of a two-layer classifier. B: Reaction schematics corresponding to each node of the classifier. C: Computationally generated input-output map of each node. Node 3 shows a nonlinear decision boundary. D: Input-output behavior observed when the output of node 3 is either the substrate or the enzyme.

sufficiently large, and can process multiple inputs with both positive and negative weights. By composing multiple layers, we can realize nonlinear classifiers in a predictable, tunable and intuitive manner. This work expands the repertoire of sequestration- and phosphorylation-based Biomolecular Neural Networks that can realize complete ideal ANNs. In vitro strand displacement Neural Networks can only be used to design linear classifiers [5], and it is challenging to assemble multi-layer neural networks to get nonlinear classifiers or to translate such circuits into living systems. PEN neural networks are challenging to implement in living systems because of the non-ideal operating conditions they require [6]. Although transcriptional-based neural networks can realize nonlinear decision making [1], [20], they do not behave as ideal perceptrons, which makes it difficult to compose multiple layers and optimize computationally. Winner-takes-all networks [10] are limited to linear classification due to the multiple interconnections that arise from each implementation. These limitations raise the open question: what are the key design principles of molecular perceptrons?

The realization of molecular perceptrons based on various mechanisms – such as sequestration [3], phosphorylation [4], and enzymatic reactions (as in this work) – suggests that endogenous networks may be able to perform pattern recog-

niton. However, the networks constructed so far lack the complexity of endogenous networks, which arises e.g. due to combinatorial binding [2], shared resources [21], and other cellular contexts. This complexity makes it challenging to evaluate how different endogenous networks are from an ideal ANN; this is a fascinating avenue for future work.

## REFERENCES

- [1] N. E. Buchler, U. Gerland, and T. Hwa, “On schemes of combinatorial transcription logic,” *Proceedings of the National Academy of Sciences*, vol. 100, no. 9, pp. 5136–5141, 2003.
- [2] Y. E. Antebi, J. M. Linton, H. Klumpe, B. Bintu, M. Gong, C. Su, R. McCardell, and M. B. Elowitz, “Combinatorial signal perception in the bmp pathway,” *Cell*, vol. 170, no. 6, pp. 1184–1196, 2017.
- [3] A. Moorman, C. C. Samaniego, C. Maley, and R. Weiss, “A dynamical biomolecular neural network,” in *2019 IEEE 58th Conference on Decision and Control (CDC)*. IEEE, 2019, pp. 1797–1802.
- [4] C. C. Samaniego, A. Moorman, G. Giordano, and E. Franco, “Signaling-based neural networks for cellular computation,” in *2021 American Control Conference (ACC)*. IEEE, 2021, pp. 1883–1890.
- [5] L. Qian, E. Winfree, and J. Bruck, “Neural network computation with dna strand displacement cascades,” *nature*, vol. 475, no. 7356, pp. 368–372, 2011.
- [6] S. Okumura, G. Gines, N. Lobato-Dauzier, A. Baccouche, R. Deteix, T. Fujii, Y. Rondelez, and A. J. Genot, “Nonlinear decision-making with enzymatic neural networks,” *Nature*, vol. 610, no. 7932, pp. 496–501, 2022.
- [7] A. Pandi, M. Koch, P. L. Voyvodic, P. Soudier, J. Bonnet, M. Kushwaha, and J.-L. Faulon, “Metabolic perceptrons for neural computing in biological systems,” *Nature communications*, vol. 10, no. 1, p. 3880, 2019.
- [8] A. A. R. Moorman, “Machine learning inspired synthetic biology: neuromorphic computing in mammalian cells,” Ph.D. dissertation, Massachusetts Institute of Technology, 2020.
- [9] R. D. Jones, Y. Qian, K. Ilija, B. Wang, M. T. Laub, D. Del Vecchio, and R. Weiss, “Robust and tunable signal processing in mammalian cells via engineered covalent modification cycles,” *Nature communications*, vol. 13, no. 1, p. 1720, 2022.
- [10] Z. Chen, J. M. Linton, R. Zhu, and M. B. Elowitz, “A synthetic protein-level neural network in mammalian cells,” *bioRxiv*, pp. 2022–07, 2022.
- [11] N. E. Buchler and M. Louis, “Molecular titration and ultrasensitivity in regulatory networks,” *Journal of molecular biology*, vol. 384, no. 5, pp. 1106–1119, 2008.
- [12] C. Briat, A. Gupta, and M. Khammash, “Antithetic integral feedback ensures robust perfect adaptation in noisy biomolecular networks,” *Cell systems*, vol. 2, no. 1, pp. 15–26, 2016.
- [13] C. C. Samaniego and E. Franco, “An ultrasensitive motif for robust closed loop control of biomolecular systems,” in *2017 IEEE 56th Annual Conference on Decision and Control (CDC)*. IEEE, 2017, pp. 5334–5340.
- [14] R. Szrednicki, “On rest points of dynamical systems,” *Fundamenta Mathematicae*, vol. 126, no. 1, pp. 69–81, 1985.
- [15] D. Richeson and J. Wiseman, “A fixed point theorem for bounded dynamical systems,” *Illinois Journal of Mathematics*, vol. 46, no. 2, pp. 491–495, 2002.
- [16] —, “Addendum to: “A fixed point theorem for bounded dynamical systems” [*Illinois J. Math.* 46(2):491–495, 2002],” *Illinois Journal of Mathematics*, vol. 48, no. 3, pp. 1079–1080, 2004.
- [17] F. Blanchini and G. Giordano, “Structural analysis in biology: a control-theoretic approach,” *Automatica*, vol. 126, p. 109376, 2021.
- [18] —, “Piecewise-linear Lyapunov functions for structural stability of biochemical networks,” *Automatica*, vol. 50, no. 10, pp. 2482–2493, 2014.
- [19] —, “Polyhedral Lyapunov functions structurally ensure global asymptotic stability of dynamical networks iff the Jacobian is non-singular,” *Automatica*, vol. 86, pp. 183–191, 2017.
- [20] L. Rizik, L. Danial, M. Habib, R. Weiss, and R. Daniel, “Synthetic neuromorphic computing in living cells,” *Nature communications*, vol. 13, no. 1, p. 5602, 2022.
- [21] Y. Qian, H.-H. Huang, J. I. Jiménez, and D. Del Vecchio, “Resource competition shapes the response of genetic circuits,” *ACS synthetic biology*, vol. 6, no. 7, pp. 1263–1272, 2017.